Accurate Ultrasonic Measurement of Surface Profile Using Phase Shift of Echo and Inverse Filtering

Chihiro Arihara, Hideyuki Hasegawa and Hiroshi Kanai*

Graduate School of Engineering, Tohoku University, Sendai 980-8579, Japan

Atherosclerosis is the main cause of circulatory diseases such as myocardial infarction and cerebral infarction, and it is very important to diagnose atherosclerosis in its early stage. In the early stage of atherosclerosis, the luminal surface of an arterial wall becomes rough because of the injury of the endothelium [R. Ross: New Engl. J. Med. **340** (2004) 115]. Conventional ultrasonic diagnostic equipments cannot detect such roughness on the order of micrometer because of their low resolution of approximately 0.1 mm. In this study, for the accurate detection of surface roughness, an ultrasonic beam was scanned in the direction that is parallel to the surface of an object. When there is a gap on the surface, the phase of the echo from the surface changes because the distance between the probe and the surface changes during the scanning. Therefore, surface roughness can be assessed by estimating the phase shift of echoes obtained during the beam scanning. Furthermore, lateral resolution, which is deteriorated by a finite diameter of the ultrasound beam, was improved by an inverse filter. By using the proposed method, the surface profile of a phantom, which had surface roughness on the micrometer order, was detected, and the estimated surface profiles became more precise by applying the inverse filter.   [DOI: 10.1143/JJAP.45.4727]

KEYWORDS: roughness, surface profile, phase shift, inverse filter, point spread function, atherosclerosis

1. Introduction

Recently, increases in the number of circulatory diseases such as myocardial infarction and cerebral infarction have become a serious problem. Therefore, it is important to diagnose atherosclerosis, which is the main cause of these diseases, in its early stage. The intima-media thickness is useful marker for the diagnosis of atherosclerosis.[1] In addition, the evaluation of the elasticity of an arterial wall is also useful for the diagnosis of early-stage atherosclerosis[2] because there are significant differences between the elastic moduli of normal arterial walls and those affected by atherosclerosis.[3,4]

We developed a method, namely, the *phased tracking method*, for measuring the regional strain and viscoelasticity of an arterial wall.[5–15] Although this method is useful for the diagnosis of atherosclerotic changes of the intima-media region, the initial step of atherosclerosis development was reported to be endothelial damage.[16] Therefore, for the diagnosis of early-stage atherosclerosis, it is more effective to initially evaluate endothelial damage. For the evaluation of endothelial function, several methods have been proposed for the evaluation of endothelium function including measurement of changes in diameter[17] and intima-media elasticity[15] caused by flow-mediated dilation. In these methods, the measured changes in diameter and elasticity are caused by the response of the media to nitric oxide generated by the endothelium. Therefore, the region where the endothelium was injured cannot be identified.

The luminal surface of a clinically healthy artery is covered by a layer of endothelial cells and it is smooth. In the early stage of atherosclerosis, endothelial cells on the luminal surface are damaged,[16] edema develops under the endothelium, endothelial cells are separated from the intima, and then the luminal surface becomes rough. There are several studies on the ultrasonic detection of the surface roughness of objects based on the characteristics of reflected echoes[18] or the three-dimensional representation of ob-jects.[19] Furthermore, there are several studies on the computer modeling of an object with a nonplanar but smooth surface.[20,21] However, this computer modeling is not yet available for an object with a rough surface.[22] To detect atherosclerosis in its early stage, the roughness of the luminal surface needs to be detected with an accuracy of micrometers that cannot be achieved by these methods. In conventional ultrasonic diagnostic equipments, the lateral interval of ultrasonic beams is approximately $100\,\mu m$, and a B-mode image is constructed using the amplitude of the received echo. Therefore, the spatial resolution of a B-mode image of an ultrasonic diagnostic equipment is $100\,\mu m$ in the lateral direction and $150\,\mu m$, which corresponds to the wavelength at 10 MHz, in the axial direction of the ultrasonic beam.

In this study, to increase the spatial resolution in the measurement of surface profile, surface roughness is evaluated using the phase of the echo from the surface of an object by scanning the ultrasonic beam with a pitch that is much smaller than the element pitch of the ultrasonic probe. When there is a gap on the surface, the phase of the received echo from the surface is changed by scanning. By estimating the phase shift of echoes obtained during the scanning, surface roughness is accurately detected in the range of $\pm75\,\mu m$ ($\pm180°$) which corresponds to the wavelength at 10 MHz. Furthermore, lateral resolution, which is deteriorated by a finite beam diameter, is improved by an inverse filter which is designed based on a point spread function[23] of the ultrasonic beam.

2. Principle

2.1 Fine beam scanning using stage

A conventional linear-type ultrasonic probe of an ultrasonic diagnostic equipment (Aloka SSD-6500) used in this study transmits and receives ultrasonic pulses by scanning with the ultrasonic beam in the direction that is parallel to the surface of an object [center frequency $f_0 = 10\,MHz$, scanning pitch $L = 0.1\,mm$, and number of electronically scanned beams $M = 70$ $(l_1, l_2, \ldots, l_m, \ldots, l_M)$]. Ultrasonic RF echoes are sampled at 40 MHz. B-mode images consist

Fig. 1. Experimental system for measurement of surface of phantom with ultrasound.

Fig. 2. Surface profile, $z(x)$, obtained by phase shift of echoes.

of sampled points, which are obtained every $19.25\,\mu m$ (sound speed $c_0 = 1{,}540\,m/s$) in the axial direction and $0.1\,mm$ in the lateral direction of the ultrasonic beam. A set of two-dimensional discrete data obtained by one scan is called a frame.

Figure 1 shows the schematic diagram of the experimental system. The depths of the object surface and the focal point were $12\,mm$ from the surface of the ultrasonic probe.

The object was measured at a frame rate of $FR = 10\,frames/s$ by moving the probe automatically using a stage at a constant speed $v_{stg} = 50\,\mu m/s$ for $2\,s$. The moving distance for $2\,s$ was $100\,\mu m$, which corresponds to the interval, L, of electronic scanning of the ultrasonic beam, in the x-direction. Let us define the location of beam l_1 in the first frame by $x(1,1) = 0\,mm$; the location, $x(k,m)$, of beam l_m at k-th frame is defined as follows:

$$x(k,m) = (m-1) \cdot L + \frac{(k-1) \cdot v_{stg}}{FR}. \qquad (2.1)$$

The probe was moved by $\Delta x = 5\,\mu m$ during a frame interval.

2.2 Detection of gaps on surface

The quadrature demodulated signal of the received RF echo was used to measure surface profile with an accuracy of micrometer-order in the axial direction of the beam. When the phase shift of the received echoes between two neighboring locations, x and $x + \Delta x$, is $\Delta\phi(x)$, which corresponds to the difference, $\Delta z(x)$, between the distances from the probe to the surface at x and that at $x + \Delta x$, surface profile, $z(x)$, is obtained as follows:

$$\Delta z(x) = \frac{c_0 \Delta\phi(x)}{4\pi f_0}, \qquad (2.2)$$

$$z(x) = \int_0^x \Delta z(x')\,dx'. \qquad (2.3)$$

Figure 2 shows the method to obtain surface profile, $z(x)$, from the phase difference of the received echoes between two neighboring locations. In the experimental system used in this paper, $\Delta z(x)$ of less than $37.5\,\mu m$, which is a quarter of the wavelength and is the aliasing limit, can be measured. In this study, the displacement of the probe in the x-axis was
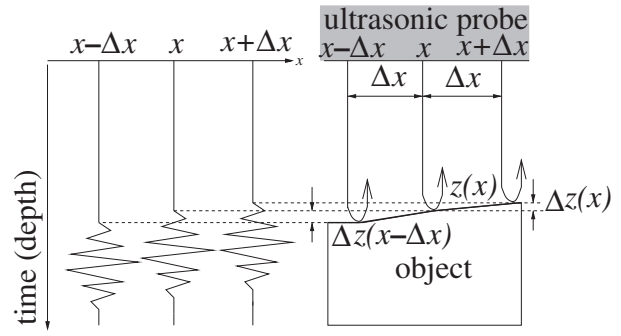
set to be much smaller than $37.5\,\mu m$ to prevent the aliasing of the estimated phase shift, $\Delta\phi(x)$.

The surface profile, $z(x)$, cannot be obtained when there are echo-lacking beam positions in the region of interest because the $\Delta z(x)$ of each of the two neighboring beams is integrated with respect to the beam position.

In this experiment, it is difficult for the surface of the ultrasonic probe to move in a direction perfectly parallel to the surface of the object. Therefore, the global angle between the surface of the ultrasonic probe and the surface of the object needs to be compensated. Angle compensated profile, $g(x)$, was obtained by subtracting the linear line, which corresponds to the global slope of the surface of the object relative to that of the probe, from the estimated $z(x)$. The linear line is obtained using the least-squares method by experimental data, $\{(x_1, z_1), (x_2, z_2), \ldots, (x_{N_{data}}, z_{N_{data}})\}$, as follows [$z_i = z(x_i)$, $i = 1, 2, \ldots, N_{data}$]:

$$g(x) = z(x) - (\hat{a}x + \hat{b}), \qquad (2.4)$$

$$\begin{pmatrix} \hat{a} \\ \hat{b} \end{pmatrix} = \frac{1}{\det}$$

$$\times \begin{pmatrix} \left(\sum_{i=1}^{N_{data}} 1\right)\left(\sum_{i=1}^{N_{data}} x_i z_i\right) - \left(\sum_{i=1}^{N_{data}} x_i\right)\left(\sum_{i=1}^{N_{data}} z_i\right) \\ \left(-\sum_{i=1}^{N_{data}} x_i\right)\left(\sum_{i=1}^{N_{data}} x_i z_i\right) + \left(\sum_{i=1}^{N_{data}} x_i^2\right)\left(\sum_{i=1}^{N_{data}} z_i\right) \end{pmatrix}, \qquad (2.5)$$

$$\det = \left(\sum_{i=1}^{N_{data}} x_i^2\right)\left(\sum_{i=1}^{N_{data}} 1\right) - \left(\sum_{i=1}^{N_{data}} x_i\right)^2, \qquad (2.6)$$

where $\hat{a}$ is the global slope of the linear line, and $\hat{b}$ is the z-intercept. N_{data} is the total number of beam positions.

2.3 Improvement of lateral resolution using inverse filter

Figure 3 shows the block diagram for estimating surface profile. Beam diameter deteriorates lateral resolution. The measured surface profile, $g(x)$, of the object is expressed by point spread function, $h(x)$, determined by the diameter of the ultrasonic beam, actual surface profile, $f(x)$, noise $n(x)$, and their Fourier spectra, $G(u)$, $H(u)$, $F(u)$, and $N(u)$, as follows:

$$g(x) = h(x) * f(x) + n(x), \qquad (2.7)$$

$$G(u) = H(u) \cdot F(u) + N(u), \qquad (2.8)$$

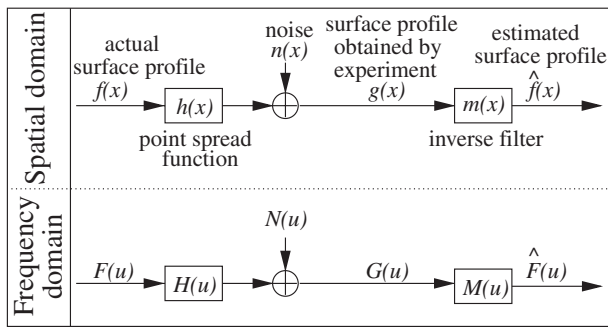where u is the spatial frequency.

Fig. 3. Block diagram for estimating surface profile, $\hat{f}(x)$.

Inverse filter, $M(u)$, is obtained by minimizing the mean squared difference between $f(x)$ shown by the model in eq. (2.7) and the estimate, $\hat{f}(x)$, as follows:[24,25]

$$M(u) = \frac{1}{H(u)} \frac{|H(u)|^2}{|H(u)|^2 + P_n(u)/P_f(u)}, \qquad (2.9)$$

where $P_n(u)$ and $P_f(u)$ are the averaged power spectra of noise and the actual surface profile, respectively. If there is no noise, $P_n(u)$ is 0 and $M(u)$ is an idealistic inverse filter.

The frequency spectrum, $\hat{F}(u)$, of the estimated surface profile, $\hat{f}(x)$, is obtained as follows:

$$\hat{F}(u) = M(u) \cdot G(u). \qquad (2.10)$$

The estimated surface profile, $\hat{f}(x)$, is obtained by the inverse Fourier transform of $\hat{F}(u)$.

3. Experimental Results

3.1 Determination of inverse filter property

The beam profile was measured by transmitting ultrasound to a stainless wire (diameter: $16\,\mu m$) and receiving the reflected echo from the wire by moving the x-position of the ultrasonic probe. When the diameter of the wire is sufficiently small compared with that of the beam, the wire is assumed to be a point scatterer. The solid line in Fig. 4(a) shows the measured beam profile, $h'(x)$. The beam width at half maximum was $500\,\mu m$. In eq. (2.8), point spread function, $h(x)$, is assumed to be noise free. Therefore, as shown by the dashed line in Fig. 4(a), Gaussian function, $p(x)$, which has the minimum root mean squared difference with respect to the measured beam profile, $h'(x)$, was used as point spread function, $h(x)$. Figure 4(b) shows the power spectrum, $|H'(u)|^2$, of the measured beam profile, $h'(x)$, and the power spectrum, $|P(u)|^2$, of Gaussian function, $p(x)$.

In addition, the signal to noise ratio $P_n(u)/P_f(u)$ must be determined. However, the power spectrum, $P_f(u)$, of the actual surface profile in a body is unknown. Therefore, the averaged surface profile, $\bar{g}(x)$, of an object obtained by 10 measurements was used as $P_f(u)$. Then, the surface profile, $g_n(x)$, of a flat object (rubber plate) was measured for 10 times to determine the magnitude of noise. Noise, $n(x)$, was defined by the difference between each $g_n(x)$ and the averaged profile, $\bar{g}(x)$, as follows:

$$\bar{g}(x) = \frac{1}{10} \sum_{n=1}^{10} g_n(x), \qquad (3.1)$$

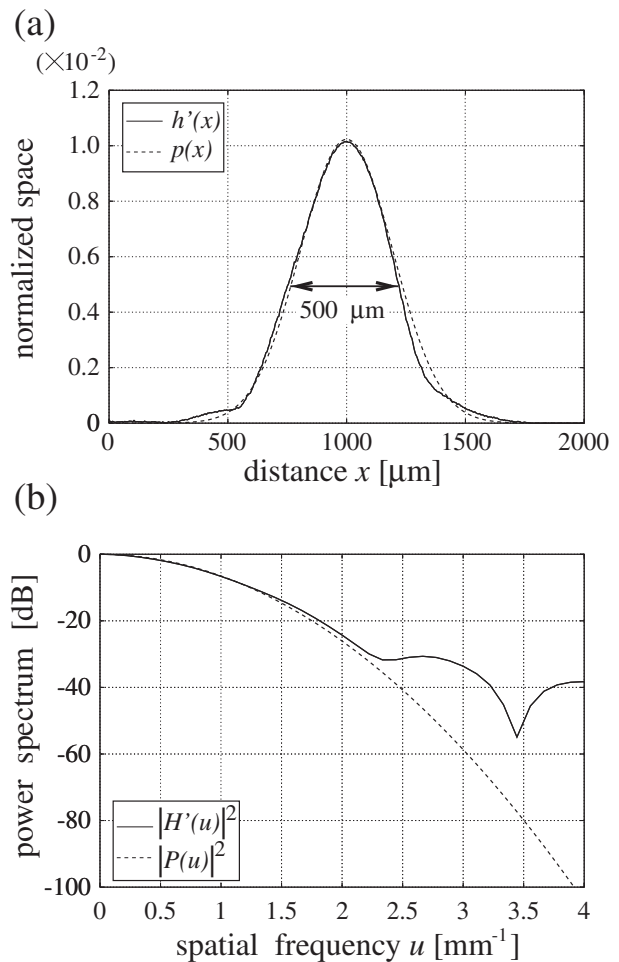$$n_n(x) = g_n(x) - \bar{g}(x). \qquad (3.2)$$

Fig. 4. (a) Measured beam profile, $h'(x)$, and Gaussian function, $p(x)$, fitted with measured beam profile, $h'(x)$. (b) Spectra of measured beam profile, $H'(u)$, and Gaussian function, $P(u)$.

The power spectrum, $P_n(u)$, of noise was defined by the mean of 10 power spectra, $|N_n(u)|^2$, of $n_n(x)$.

$$P_n(u) = \frac{1}{10} \sum_{n=1}^{10} |N_n(u)|^2. \qquad (3.3)$$

3.2 Results of basic experiments

An object made of silicone rubber was placed in a water tank. Figure 5(b) shows the surface profile along a black line shown in Fig. 5(a). The surface profile shown in Fig. 5(b) was measured using a surface profilometer.

Power spectra, $P_n(u)$, $P_f(u)$, $|H(u)|^2$, and $|M(u)|^2$, obtained by the above procedure are shown in Fig. 6. $|M(u)|^2$ was positive in a spatial frequency range of less than $2.0\,mm^{-1}$, and negative over $2.0\,mm^{-1}$. The signal was increased in a spatial frequency of less than $2.0\,mm^{-1}$, and was decreased over $2.0\,mm^{-1}$. The inverse filter, $|M(u)|^2$, had the reciprocal property of the spectrum, $H(u)$, of the point spread function in the frequency range where $P_n(u)/P_f(u)$ was low.

Figure 7(a) shows a B-mode image obtained by the ultrasonic diagnostic equipment. Figure 7(b) shows the measured surface profile, $g(x)$, of the object in the region of interest surrounded by the white line in Fig. 7(a). A gap,
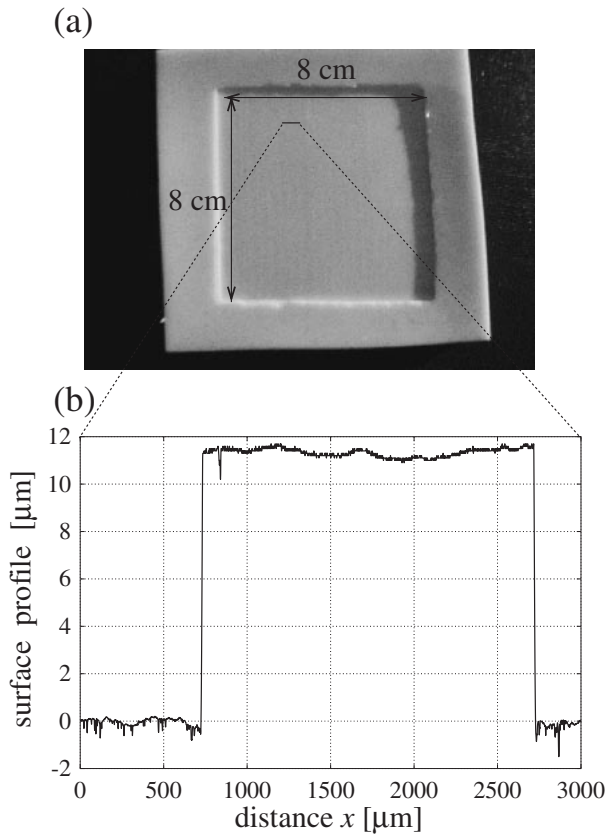
(a)

8 cm

8 cm

(b)

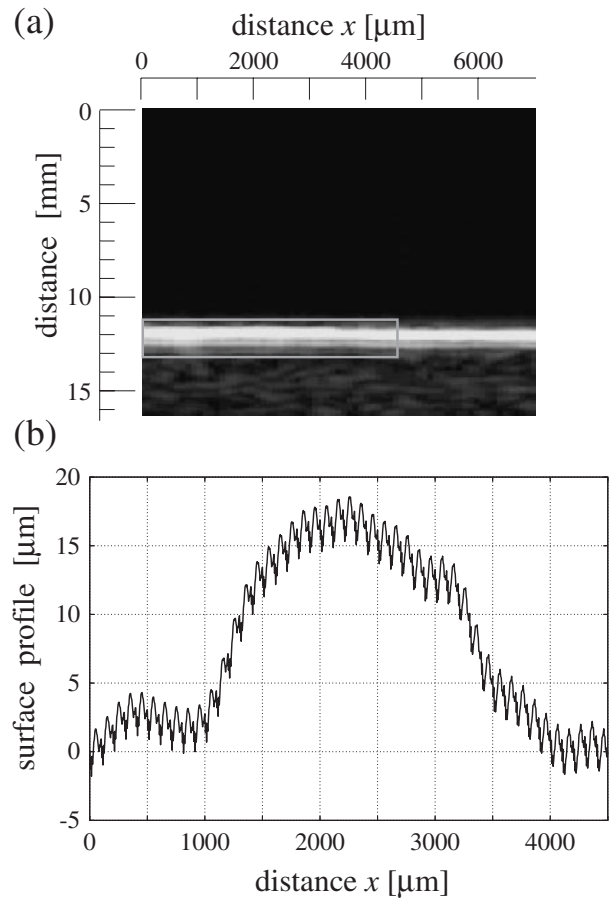Fig. 5.   (a) Image of object made of silicone rubber. (b) Surface profile of object measured by bump instrument.
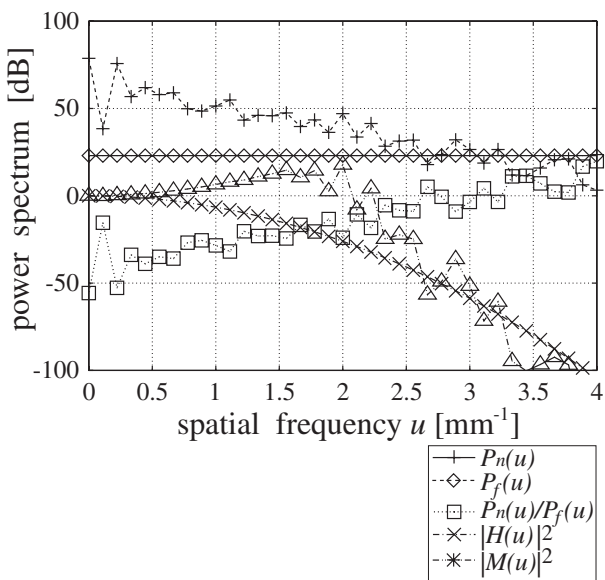

Fig. 6.   Inverse filter property.

which could not be recognized in Fig. 7(a), could be found easily in Fig. 7(b). The spatial resolution in Fig. 7(b) was much improved in comparison with that of the conventional B-mode image. Comparing Fig. 7(b) with Fig. 5(b), the width and height of the gap found in $g(x)$ were similar to the actual surface profile of the object (width: 2,000 μm, height: 12 μm). Cyclical noise shown in $g(x)$ of Fig. 7(b) was caused

(a)

(b)

Fig. 7.   (a) B-mode image. (b) Measured surface profile, $g(x)$.

by the vertical motion of the probe because of the motion of the automatic stage.

Figure 8(a) shows surface profiles, $g(x)$ and $\hat{f}(x)$. The estimate, $\hat{f}(x)$, of the surface profile was obtained after applying the inverse filter to $g(x)$. After inverse filtering, the surface profile became steeper and the upper base of the trapezoidal shape became almost flat. Figure 8(b) shows the power spectra of surface profiles, $g(x)$ and $\hat{f}(x)$. After inverse filtering, spatial frequency components less than $2.0\,\mathrm{mm}^{-1}$, which sharpened the estimated surface profile, $\hat{f}(x)$, were increased, and the undesirable components over $2.0\,\mathrm{mm}^{-1}$, which are caused by movement of the stage, were reduced. The estimated surface profile, $\hat{f}(x)$, had ripples. This phenomenon called the Gibbs phenomenon occurs by forcing high frequency components to be removed in the Fourier analysis. Window function is generally used to reduce the ripples by the Gibbs phenomenon. However, in this study, a rectangular window was used to avoid the deformation of the surface profile, $g(x)$.

4.   Conclusions

In this study, the surface profile of an object made of silicone rubber on the micrometer order was measured using the phase of an RF echo. By applying an inverse filter that was designed on the basis of the point spread function of an ultrasonic beam to the measured surface profile, the estimated surfaces became more precise than the measured surface profiles without the inverse filter.
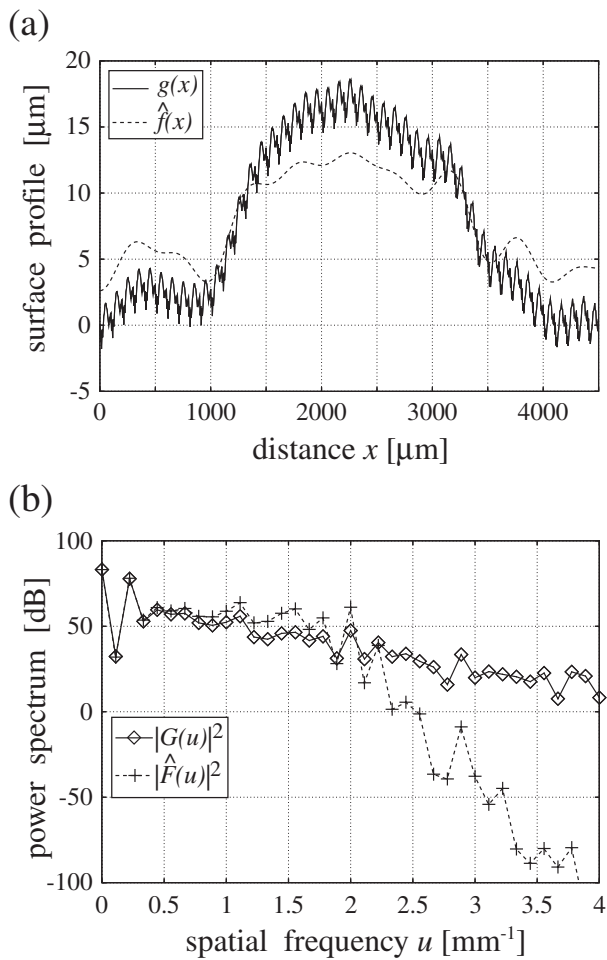
(a)

(b)

Fig. 8. (a) Surface profiles, $g(x)$ and $\hat{f}(x)$. (b) Power spectra of surface profiles, $g(x)$ and $\hat{f}(x)$.

1) I. Wendelhag, O. Wiklund and J. Wikstrand: Arterioscler. Thromb. Vasc. Biol. **16** (1996) 843.
2) P. C. G. Simons, A. Algra, M. L. Bots, D. E. Grobbee and Y. van der Graaf: Circulation **100** (1999) 951.
3) R. T. Lee, A. J. Grodzinsky, E. H. Frank, Roger D. Kamm and F. J. Schoen: Circulation **83** (1991) 1764.
4) H. M. Loree, A. J. Grodzinsky, S. Y. Park, L. J. Gibson and R. T. Lee: J. Biomech. **27** (1994) 195.
5) H. Kanai, M. Sato, Y. Koiwa and N. Chubachi: IEEE Trans. Ultrason. Ferroelectr. Freq. Control **43** (1996) 791.
6) H. Hasegawa, H. Kanai, N. Hoshimiya and Y. Koiwa: Jpn. J. Appl. Phys. **39** (2000) 3257.
7) H. Hasegawa, H. Kanai and Y. Koiwa: Jpn. J. Appl. Phys. **41** (2002) 3563.
8) H. Kanai, H. Hasegawa, M. Ichiki, F. Tezuka and Y. Koiwa: Circulation **107** (2003) 3018.
9) H. Hasegawa, H. Kanai, Y. Koiwa and J. P. Butler: Jpn. J. Appl. Phys. **42** (2003) 3255.
10) H. Hasegawa and H. Kanai: Jpn. J. Appl. Phys. **43** (2004) 3197.
11) N. Nakagawa, H. Hasegawa and H. Kanai: Jpn. J. Appl. Phys. **43** (2004) 3220.
12) J. Tang, H. Hasegawa and H. Kanai: Jpn. J. Appl. Phys. **44** (2005) 4588.
13) J. Inagaki, H. Hasegawa, H. Kanai, M. Ichiki and F. Tezuka: Jpn. J. Appl. Phys. **44** (2005) 4593.
14) H. Hasegawa and H. Kanai: Jpn. J. Appl. Phys. **44** (2005) 4609.
15) M. Sugimoto, H. Hasegawa and H. Kanai: Jpn. J. Appl. Phys. **44** (2005) 6297.
16) R. Ross: New Engl. J. Med. **340** (2004) 115.
17) M. Hashimoto, M. Akishita, M. Eto, M. Ishikawa, K. Kozaki, K. Toba, Y. Sagara, Y. Taketani, H. Orimo and Y. Ouchi: Circulation **92** (1995) 3431.
18) J. E. Wilhjelm, P. C. Pedersen, S. M. Jacobsen and K. Martinsen: Proc. IEEE Ultrasonic Symp., 1998, p. 5.
19) W. Y. Zhang, R. N. Rohling and D. K. Pai: Ultrasound Med. Biol. **30** (2004) 1461.
20) P. C. Pedersen and D. P. Orofino: IEEE Trans. Ultrason. Ferroelectr. Freq. Control **43** (1996) 303.
21) S. K. Jespersen, P. C. Pendersen and J. E. Wilhjelm: IEEE Trans. Ultrason. Ferroelectr. Freq. Control **45** (1998) 1461.
22) B. J. Dean and P. C. Pedersen: Proc. IEEE Ultrasonic Symp., 1996, Vol. 3, p. 693.
23) N. B. Jones: *Digital Signal Processing* (Short Run Press, Tokyo, 1982) p. 287.
24) H. C. Andrews and B. R. Hunt: *Digital Image Restoration* (Prentice-Hall, New Jersey, 1977) p. 126.
25) W. K. Pratt: *Digital Image Processing* (John Wiley & Sons, New York, 1978) p. 410.